Differential sampling of visual space in ventral and dorsal early visual cortex

Systems/Circuits

Differential Sampling of Visual Space in Ventral and Dorsal Early Visual Cortex

Edward H. Silson,[1] Richard C. Reynolds,[2] Dwight J. Kravitz,[3]* and Chris I. Baker[1]*

[1]Section on Learning and Plasticity, Laboratory of Brain and Cognition, [2]Scientific and Statistical Computing Core, National Institute of Mental Health, Bethesda, Maryland 20892, and [3]Department of Psychology, The George Washington University, Washington DC 20052

A fundamental feature of cortical visual processing is the separation of visual processing for the upper and lower visual fields. In early visual cortex (EVC), the upper visual field is processed ventrally, with the lower visual field processed dorsally. This distinction persists into several category-selective regions of occipitotemporal cortex, with ventral and lateral scene-, face-, and object-selective regions biased for the upper and lower visual fields, respectively. Here, using an elliptical population receptive field (pRF) model, we systematically tested the sampling of visual space within ventral and dorsal divisions of human EVC in both male and female participants. We found that (1) pRFs tend to be elliptical and oriented toward the fovea with distinct angular distributions for ventral and dorsal divisions of EVC, potentially reflecting a radial bias; and (2) pRFs in ventral areas were larger (~1.5×) and more elliptical (~1.2×) than those in dorsal areas. These differences potentially reflect a tendency for receptive fields in ventral temporal cortex to overlap the fovea with less emphasis on precise localization and isotropic representation of space compared with dorsal areas. Collectively, these findings suggest that ventral and dorsal divisions of EVC sample visual space differently, likely contributing to and/or stemming from the functional differentiation of visual processing observed in higher-level regions of the ventral and dorsal cortical visual pathways.

Key words: population receptive field modeling; retinotopy; visual cortex

Significance Statement

The processing of visual information from the upper and lower visual fields is separated in visual cortex. Although ventral and dorsal divisions of early visual cortex (EVC) are commonly assumed to sample visual space equivalently, we demonstrate systematic differences using an elliptical population receptive field (pRF) model. Specifically, we demonstrate that (1) ventral and dorsal divisions of EVC exhibit diverging distributions of pRF angle, which are biased toward the fovea; and (2) ventral pRFs exhibit higher aspect ratios and cover larger areas than dorsal pRFs. These results suggest that ventral and dorsal divisions of EVC sample visual space differently and that such differential sampling likely contributes to different functional roles attributed to the ventral and dorsal pathways, such as object recognition and visually guided attention, respectively.

Introduction

One prominent feature of the cortical visual pathways is the segregated processing of input from the upper and lower visual field. In early visual cortex (EVC; V1–V3), the upper visual field is processed ventrally and the lower visual field is processed dorsally (Wandell et al., 2007). This distinction persists into higher-level visual areas with scene-, face-, and object-selective regions in ventral occipitotemporal cortex biased for the upper visual field and those in lateral regions biased for the lower visual field (Arcaro et al., 2009; Kravitz et al., 2010; Silson et al., 2015, 2016). While it is commonly assumed that ventral and dorsal divisions of EVC sample visual space equivalently, evidence suggests potential differences. First, functional differentiation between the upper and lower visual fields has been reported in retinal ganglion cell densities (Packer et al., 1989; Curcio and Allen, 1990; Curcio et al., 1990). Second, ventral and dorsal divisions of V2 and V3 contain different GABA receptor concentrations (Eickhoff et al., 2008), perhaps reflecting different functional properties and helping to explain behavioral differences for the upper and lower visual fields. For example, stimulus discrimination and change detection advantages have been reported in the upper visual field (Rutkowski et al., 2002; Levine and McAnany, 2005), whereas advantages in visually guided pointing, spatial recollection memory, and attentional resolution (He, et al., 1996;

Received Sept. 20, 2017; revised Jan. 8, 2018; accepted Jan. 11, 2018.

Author contributions: E.H.S., R.C.R., D.J.K., and C.I.B. designed research; E.H.S. performed research; E.H.S., R.C.R., D.J.K., and C.I.B. analyzed data; E.H.S., D.J.K., and C.I.B. wrote the paper.

*D.J.K. AND C.I.B. share senior authorship.

We thank Iris Groen, Martin Hebert, Eli Merriam, Alexis Kidder, and members of the Section on Learning and Plasticity for helpful comments on earlier versions of the manuscript.

Correspondence should be addressed to Edward H. Silson, Section on Learning and Plasticity, Laboratory of Brain and Cognition, National Institute of Mental Health, Bethesda, MD 20892. E-mail: ed.silson@nih.gov.

DOI:10.1523/JNEUROSCI.2717-17.2018

 0270-6474/18/382294-10$15.00/0

Danckert and Goodale, 2001; Genzano et al., 2001) have been reported in the lower visual field. Further, differential effects of attention between the upper and lower visual fields have been shown to reflect the larger extent of the lower compared with the upper visual field as well as individual differences in the shape and extent of those fields (Fortenbaugh et al., 2015).

Here, using functional magnetic resonance imaging (fMRI), we examined differences in the sampling of visual space within ventral and dorsal divisions of human EVC using population receptive field (pRF) modeling. The majority of previous pRF studies model the pRF of a voxel as a circular aperture defined by its centroid (x, y) and size (σ; Dumoulin and Wandell, 2008; Harvey et al., 2013; Silson et al., 2015, 2016), although more recent studies also model suppressive surrounds (Zuiderbaan et al., 2012) and subadditive spatial summation (Kay et al., 2013). However, given the evidence for elongated receptive fields of individual neurons (Hubel and Wiesel, 1962) and populations of neurons (Yoshor et al., 2007), a more biologically plausible model would allow for pRFs to take an elliptical shape as a circular pRF assumes that orientations of neuronal receptive fields within a voxel are distributed evenly. Indeed, a model-free pRF approach (Greene et al., 2014) reported some deviation from circular pRFs, with ~11% of EVC voxels (<3.5°) exhibiting an aspect ratio (AR) of >2.

First, we predicted that elliptical pRFs would be oriented toward fovea. Specifically, a radial bias has been reported within EVC (Sasaki et al., 2006), with fMRI activity ~20% higher in the retinotopic representations of polar angle (upper/lower quadrant maps) that corresponded to radial stimulus orientations. Further, a coarse-scale orientation map has been identified in V1 whereby the orientation sensitivity of a given voxel was largely commensurate with its preferred polar angle (Freeman et al., 2011).

Second, we predicted that pRFs in ventral division of EVC would be more elliptical (larger aspect ratio) and cover a larger area than those in dorsal division of EVC. The ventral division of EVC is strongly associated with the ventral visual pathway (Kravitz et al., 2013), which is often characterized by an overrepresentation of the fovea. For example, neurons in macaque inferior temporal cortex exhibit receptive fields that typically overlap the fovea (Op de Beeck and Vogels, 2000) regardless of eccentricity. In contrast, the dorsal division of EVC is more associated with the dorsal visual pathway, which has a more isotropic representation of space (Gattass et al., 2005; Sheth and Young, 2016). While these differences in higher-order areas could reflect a selective sampling of EVC, here we tested whether such differential sampling of space emerges within EVC.

Materials and Methods

Participants and testing. Twelve participants in total (five females; mean age, 29 years) completed the fMRI experiments. All participants had normal or corrected-to-normal vision, and gave written informed consent. The National Institutes of Health Institutional Review Board approved the consent and protocol. (This work was supported by the Intramural Research Program of the National Institutes of Health–National Institute of Mental Health Clinical Study Protocol 93-M-0170, NCT00001360.)

fMRI scanning parameters. Participants were scanned using either a research-dedicated GE Healthcare 3 tesla SIGNA Scanner (eight participants) or a research-dedicated Siemens 7 tesla Magnetom Scanner (four participants) in the Clinical Research Center on the National Institutes of Health campus (Bethesda, MD). In all scans and across scanners, oblique slices were oriented approximately parallel to the base of the temporal lobe and extended posteriorly through all of visual cortex.

3 T scanning parameters. Partial volumes of the occipital and temporal cortices were acquired using an eight-channel head coil (21 slices; 2 × 2 × 2 mm; 10% interslice gap; TR, 2 s; TE, 30 ms; matrix size, 96 × 96; FOV, 192 mm).

7 T scanning parameters. Partial volumes of the occipital and temporal cortices were acquired using a 32-channel head coil (42 slices; 1.2 × 1.2 × 1.2 mm; 10% interslice gap; TR, 2 s; TE, 27 ms; matrix size, 170 × 170; FOV, 192 mm).

Visual stimuli and tasks. During pRF mapping sessions, a bar aperture traversed gradually through the visual field while revealing randomly selected scene fragments from a total of 90 color images. During each 36 s sweep, the aperture took 18 evenly spaced steps every 2 s (1 TR) to traverse the entire screen. At each bar position, five scene fragments were displayed in rapid succession (400 ms/image). Across the 18 aperture positions, all 90 possible scene images were displayed once. A total of eight sweeps were made during each run (four orientations, two directions). Specifically, the bar aperture progressed in the following order for all runs: left to right, bottom right to top left, top to bottom, bottom left to top right, right to left, top left to bottom right, bottom to top, and top right to bottom left. The bar stimuli covered a circular aperture (20° diameter 7 T, individual bar width = 1.6°; 15° diameter 3 T, individual bar width = 1.25°). Participants performed a color detection task at fixation, indicating via button press when the white fixation dot changed to red. Color fixation changes occurred semirandomly, with approximately two color changes per sweep (Silson et al., 2015).

fMRI data preprocessing. All data were analyzed using the Analysis of Functional NeuroImages (AFNI) software package (Cox, 1996; http://afni.nimh.nih.gov/afni). Before statistical and pRF analyses, all images for each participant were motion corrected to the first image of the first run, after removal of the appropriate "dummy" volumes (eight volumes) to allow stabilization of the magnetic field.

pRF modeling. pRF analyses were conducted in AFNI. Unlike our own work (Silson et al., 2015, 2016) and previous work by others (Dumoulin and Wandell, 2008; Harvey et al., 2013), which used variants of a 2-D Gaussian model, we used a pRF implementation that models elliptical pRFs.

Given the position of the stimulus in the visual field at every time point, the model estimates the pRF parameters that yield the best fit to the data: pRF center location (x, y), ratio of the major to minor widths (aspect ratio), and the orientation of the major axis (angle). Both Simplex and Powell optimization algorithms are used simultaneously to find the best time series/parameter sets (x, y, aspect ratio, and angle) by minimizing the least-squares error of the predicted time series measured against the acquired time series in each voxel. All functions and programs are available in the current version of AFNI (3dNLfim AFNI_17.1.10; compiled June 6, 2017).

Delineation of visual field maps. To identify EVC in individual participants, the representations of polar angle and eccentricity were visualized on surface reconstructions of both hemispheres and inspected. Surface reconstructions of the gray and white matter boundary of individual participant hemispheres were made using the Freesurfer4 autorecon script (http://surfer.nmr.mgh.harvard.edu/).

Retinotopically organized maps were visible and present in all tested hemispheres. Notwithstanding subtle interparticipant variability, the main features of the maps, in particular the reversals in visual field representation at the vertical and horizontal

meridians were consistent across participants. In accordance with previous reports (DeYoe et al., 1994; Sereno et al., 1995; Engel et al., 1997; Larsson and Heeger, 2006; Wandell et al., 2007), visual field maps (VFMs) were delineated using the following criteria: (1) the polar angle representations displayed reversals. That is, representations of polar angle in neighboring visual areas were mirror reversals of one another, with a reversal in the representation along their shared boundary; (2) the polar angle and eccentricity components within each visual area were organized largely orthogonal to one another. The following visual field maps were identified in each hemisphere and participant (V1, V2d, V2v, V3d, V3v). To divide V1 into ventral (V1v) and dorsal (V1d) divisions, we selected nodes with an angular position above and below the horizontal meridian, respectively. Importantly, these maps were defined relative to the polar coordinate of pRF centroids only, without reference to the size, eccentricity, aspect ratio, or angle of the pRF.

Reliability analyses. Before comparing differences between ventral and dorsal divisions of EVC, we tested the reliability of our elliptical pRF parameter estimates by splitting the eight pRF runs for each participant into odd and even runs (four runs each) and analyzing these now independent datasets with both circular and elliptical pRF models.

Initially, we compared the reliability of our elliptical estimates with those derived from the circular pRF method in a cross-validated approach. For each participant and split (odd/even), we compared how well the estimated time series predicted the time series in the independent dataset. For each voxel, we correlated (Pearson's correlation coefficient) the predicted time series from the odd runs with the actual time series in the even runs and squared the resulting correlation value. This process was reversed, and the average was computed. We then computed the difference in cross-validated explained variance (R^2) for each participant between elliptical and circular pRF models.

Next, the elliptical pRF parameter estimates (x, y, aspect ratio, and angle) derived for each set of runs in our elliptical model were compared on a node-wise basis in each participant, collapsing across visual field maps V1 to V3. Initially, we selected significantly modulated nodes ($R^2 > 0.2$) in the odd runs and correlated the parameters of interest with the parameters extracted from the exact nodes in the even runs. This process was reversed to avoid any bias in node selection, and the average was computed. Of note, due to the circular nature of angle estimates we computed the odd/even correlation of angle using a circular correlation coefficient method.

Statistical analyses. Statistics were calculated using the SPSS software package (version 24; IBM). For our analyses, we used repeated-measures ANOVAs to examine differences in our pRF parameters between ventral and dorsal divisions of EVC. For each analysis, we established initially whether the ANOVA adhered to the assumptions of sphericity using Mauchly's test. When the assumption of sphericity was violated, the degrees of freedom for the offending main effect or interaction were corrected using the Greenhouse–Geisser correction to allow appropriate interpretation of the F value resulting from the ANOVA.

Results

We used an elliptical pRF model to test the prediction that ventral and dorsal divisions of EVC differentially sample visual space (Fig. 1, group average pRF parameters on the cortical surface). Before systematically comparing ventral and dorsal divisions of EVC, we established the reliability of the elliptical pRF estimates.

Reliability of elliptical pRF estimates

Initially, we compared the explained variance between the elliptical and circular pRF models using a cross-validated approach (see Reliability analyses). On average, we observed a significant advantage for the elliptical model ($t_{(11)} = 2.10, p = 0.03$), with an elliptical advantage in all but one participant, reflecting that our elliptical pRF model captures significantly more of the variance in the time courses than the circular model.

Next, we examined the reliability of our elliptical pRF parameters. For each parameter, we compared both the correlation (Pearson's correlation coefficient) as well as the absolute differences between independent estimates (see Reliability analyses). For each parameter, there were no significant differences in either Pearson's correlation coefficient between hemispheres [paired t test (two-tailed), x ($t_{(11)} = 0.22$, $p = 0.82$); y ($t_{(11)} = 0.05$, $p = 0.95$); aspect ratio ($t_{(11)} = 0.05$, $p = 0.95$); angle ($t_{(11)} = 0.13$, $p = 0.89$)] or the absolute differences between hemispheres [paired t test (two-tailed), x ($t_{(11)} = 0.10$, $p = 0.91$); y ($t_{(11)} = 0.23$, $p = 0.81$); aspect ratio ($t_{(11)} = 0.06$, $p = 0.95$); angle ($t_{(11)} = 0.73$, $p = 0.47$)], so for further analyses we collapsed across hemispheres.

We observed significant positive correlations for all parameters (t test relative to zero (two-tailed), [x ($t_{(11)} = 42.07$, $p = 1.66^{-13}$); y ($t_{(11)} = 33.3$, $p = 2.13^{-12}$); aspect ratio ($t_{(11)} = 27.92$, $p = 1.45^{-11}$); angle ($t_{(11)} = 15.84$, $p = 6.40^{-9}$); Fig. 2*A*]. The lowest correlation was for pRF angle, but it is important to consider the influence of aspect ratio. A pRF with an aspect ratio near 1 will result in an unstable estimate of angle, as the principle axis could take a different orientation with little loss in explained variance. We therefore tested the prediction that our estimates of angle would become increasingly reliable with increasing aspect ratio. Accordingly, we computed the correlation between odd and even angle estimates for pRFs that fell into one of four aspect ratio bins (1–2, 2–3, 3–4, and 4–5; Fig. 2*B*). With increasing aspect ratio, the correlation of the angle estimates increased. A one-way repeated-measures ANOVA with aspect ratio as a within-subjects factor revealed a significant main effect of aspect ratio ($F_{(3, 33)} = 2.83$, $p = 0.05$), reflecting the increase in reliability as a function of increasing aspect ratio.

We also computed the distribution of the absolute differences in each parameter between odd and even runs. In each case, the absolute differences were small (mean ± SD: $x = 0.78° \pm 0.01°$; $y = 0.73° \pm 0.01°$; aspect ratio = 0.05 ± 0.07; angle = $14.35° \pm 1.35°$; across all AR bins: AR1–2 = $15.4° \pm 1.51°$; AR2–3 = $14.14° \pm 1.35°$; AR3–4 = $13.94° \pm 1.23°$; AR4–5 = $13.63° \pm 1.3°$), which reflects the reliability of our pRF parameter estimates across independent runs (Fig. 2*C*).

Ventral and dorsal pRFs are oriented toward the fovea

Our first prediction was that due to the restricted representations within ventral (upper visual field) and dorsal (lower visual field) divisions of EVC, and the presence of both a coarse-scale orientation map (Freeman et al., 2011) and radial biases (Sasaki et al., 2006), pRFs would exhibit a general orientation bias toward the fovea. In particular, if 0° represents the horizontal axis with positive angles toward the upper vertical meridian and negative angles toward the lower vertical meridian, we hypothesized that ventral regions (V1v, V2v, and V3v) would show a positively biased distribution of pRF angles, with dorsal regions (V1d, V2d, and V3d) exhibiting the opposite bias, largely commensurate with their visual field representations. Our results reveal a striking difference in the distributions of pRF angle within ventral and dorsal divisions of V2 and V3, consistent with these predictions

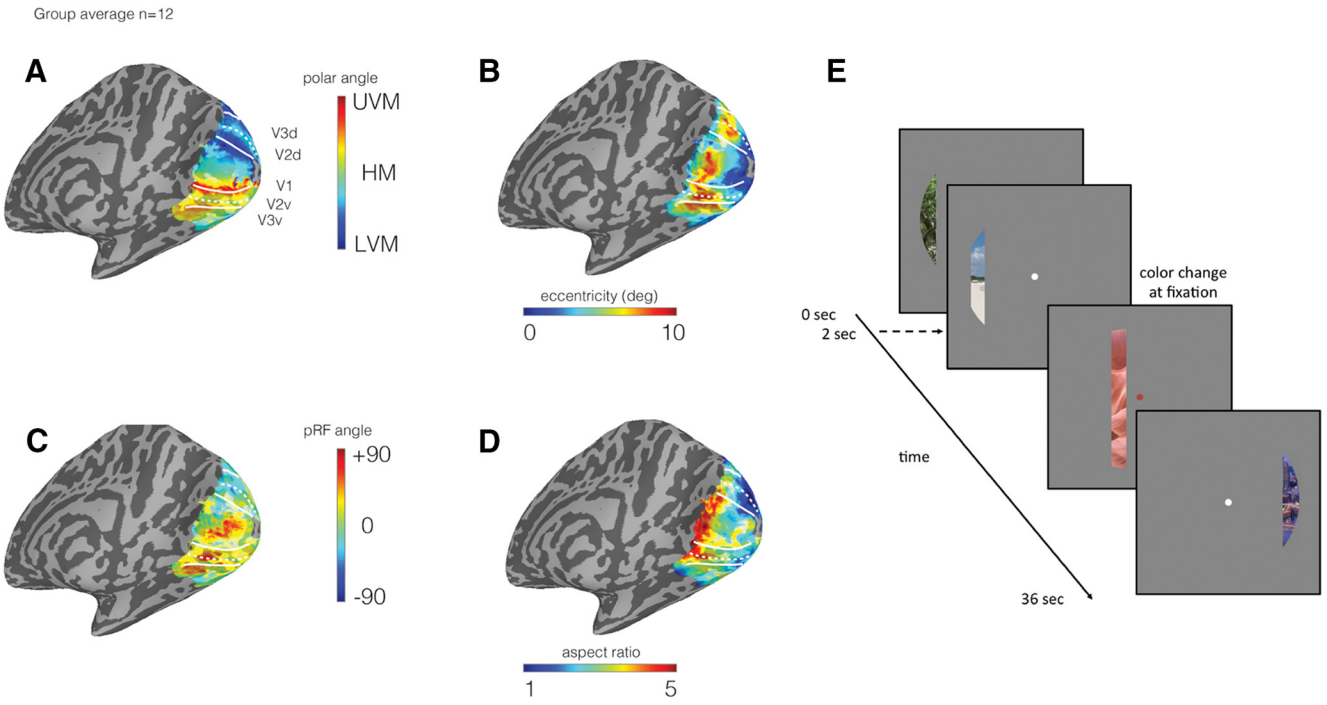

Figure 1. Distribution of pRF parameters across the cortical surface. ***A***, A medial view of the surface reconstruction of the right hemisphere of a single participant is shown (gyri are light gray, sulci are dark gray). The group average ($n = 12$) polar angle is overlaid in false color ($R^2 > 0.2$). Red and blue represent the upper vertical meridian (UVM) and lower vertical meridian (LVM), respectively, with the horizontal meridian (HM) represented by green. The borders defining EVC (V1, V2d, V2v, V3d, and V3v) are overlaid in white, with the horizontal meridian borders represented by the dashed line. The polar angle representations follow predicted patterns with lower visual field representations dorsally and upper visual field representations ventrally. ***B***, Eccentricity is overlaid in false color. Blue represents central positions in the visual field with red representing the periphery. The progression of eccentricity follows a well established and predicted pattern, progressing gradually from central representations at the occipital pole, to peripheral representations more anteriorly. ***C***, Estimates of pRF angle are overlaid in false color. Negative (lower visual field) angles are shown in green/blue colors, and positive (upper visual field) angles are shown in red. Although the organization of the pRF angle is not as smooth as the polar angle, there is a general tendency for negative angles more dorsally (lower visual field representaitons in ***A***), and positive angles more ventrally (upper visual field representations in ***B***). ***D***, Estimates of pRF aspect ratio are overlaid in false color. Circular pRFs (aspect ratio, 1) are shown in blue, with very elliptical pRFs (aspect ratio, 5:1) shown in red. Although the organization of pRF aspect ratio across the cortical surface is not as smooth as eccentricity, there is a general tendency for more circular (lower aspect ratios) pRFs to be located more posteriorly (central representations in ***B***), with very elliptical pRFs (higher aspect ratios) more anteriorly (peripheral representations in ***B***). ***E***, Schematic of pRF mapping stimulus. Example frames during pRF mapping runs. Scene images (one every 400 ms) were presented through a bar aperture that moved gradually through the visual field in eight sweeps (2 orientations, 4 directions). A single sweep took 36 s and consisted of 18 equal time (2 s) and width instances of the aperture. Over an entire sweep, 90 scene images (5×18 aperture positions) were presented at random without replacement, guaranteeing that no scene was presented twice during a sweep. Participants fixated centrally, identifying via button press every time the fixation dot changed from white to red (approximately twice per sweep). Error bars show the standard error of the mean (SEM) across participants.

(Fig. 3). Initially, we tested for hemispheric differences in the distribution of the pRF angle within each visual field map division using two-sample Kolmogorov–Smirnov (KS) tests (two-tailed). There were no significant differences between hemispheres for any visual field map division [V1v (ks = 0.07, $p = 0.99$); V1d (ks = 0.07, $p = 0.99$); V2v (ks = 0.07, $p = 0.99$); V2d (ks = 0.15, $p = 0.61$); V3v (ks = 0.11, $p = 0.92$); V3d (ks = 0.09, $p = 0.99$)]; thus, distributions of pRF angle were averaged across hemispheres. Next, we compared directly the ventral and dorsal divisions for each visual field map separately using two-sample KS tests. There were significant differences between the pRF angle distributions of ventral and dorsal V2 (KS = 0.15, $p = 0.03$) and V3 (KS = 0.22, $p = 0.002$), respectively, although ventral and dorsal V1 were not significantly different (KS = 0.06, $p = 0.98$). In the case of V2 and V3, ventral maps exhibited a positively biased angle distribution, with dorsal maps exhibiting a negatively biased angle distribution largely commensurate with their visual field representations (Fig. 3).

Ventral pRFs are more elliptical than dorsal pRFs

Along with diverging orientations, we also predicted that ventral pRFs would be more elliptical than their dorsal counterparts. Potentially reflecting the importance of the fovea often attributed to anterior regions of the ventral pathway and of a more even and precise representation of space in the dorsal pathway, both of which receive major input from ventral and dorsal EVC divisions, respectively (Kravitz et al., 2013). To test this, we initially computed the distribution of aspect ratios in each participant and visual field map division. First, we tested for hemispheric differences within each visual field map division using two-sample KS tests (two-tailed). There were no significant differences between hemispheres for any visual field map [V1v (ks = 0.06, $p = 1.00$); V1d (ks = 0.06, $p = 1.00$); V2v (ks = 0.06, $p = 1.00$); V2d (ks = 0.06, $p = 1.00$); V3v (ks = 0.10, $p = 0.96$); V3d (ks = 0.06, $p = 1.00$)]; thus, distributions of aspect ratio were averaged across hemispheres (Fig. 4). Next, we compared directly each ventral and dorsal division separately using two-sample KS tests. There were significant differences between the aspect ratio distributions of ventral and dorsal V2 (ks = 0.24, $p = 0.05$) and V3 (ks = 0.25, $p = 0.03$), but not V1 (ks = 0.10, $p = 0.47$), despite a similar overall pattern. Across visual field maps, the distributions of aspect ratio in dorsal divisions were shifted toward smaller aspect ratios (more circular), with ventral divisions showing broader distributions.

Next, we computed the median aspect ratio in each participant and visual field map separately. Across participants, the

mean aspect ratio was larger in ventral than dorsal divisions of EVC (Fig. 5*A*). A three-way repeated-measures ANOVA with within-participant factors of VFM (V1, V2 and V3), division (ventral, dorsal), and hemisphere (left, right) revealed a significant main effect of the VFM ($F_{(2,22)} = 41.86, p = 3.16^{-8}$), reflecting on average larger aspect ratios in V1. The main effect of division was also significant ($F_{(1,11)} = 33.49, p = 0.0001$), reflecting on average larger aspect ratios in ventral over dorsal divisions within each region. These main effects, however, are qualified by a significant VFM by division interaction ($F_{(1,11)} = 3.25$, $p = 0.058$). No interactions were significant ($p > 0.05$, in all cases).

To determine what is driving this interaction, we computed three separate two-way ANOVAs for each pair of regions, with VFM and division as within-participant factors. Given the lack of a significant main effect of hemisphere ($F_{(1,11)} = 0.12$, $p = 0.74$), aspect ratios were averaged across hemispheres. These analyses revealed that the ventral/dorsal difference in aspect ratio was significantly different between V1 and both V2 and V3, but not between V2 and V3 [V1 to V2, VFM by division ($F_{(1,11)} = 19.96$, $p = 0.001$); V1 to V3, VFM by division ($F_{(1,11)} = 28.47$ $p = 0.0002$); V2 to V3, VFM by division ($F_{(1,11)} = 0.15, p = 0.70$]. We then compared directly the mean aspect ratios within ventral and dorsal divisions of EVC using paired *t* tests (one-tailed). Consistent with our predictions, ventral aspect ratios were significantly larger than dorsal aspect ratios in each VFM [V1v vs V1d ($t_{(11)} = 4.47, p = 0.0001$); V2v vs V2d ($t_{(11)} = 4.05$, $p = 0.0002$); V3v vs V3d ($t_{(11)} = 5.62$, $p = 0.00007$); Fig. 5*A*], with a larger difference in the further anterior regions.

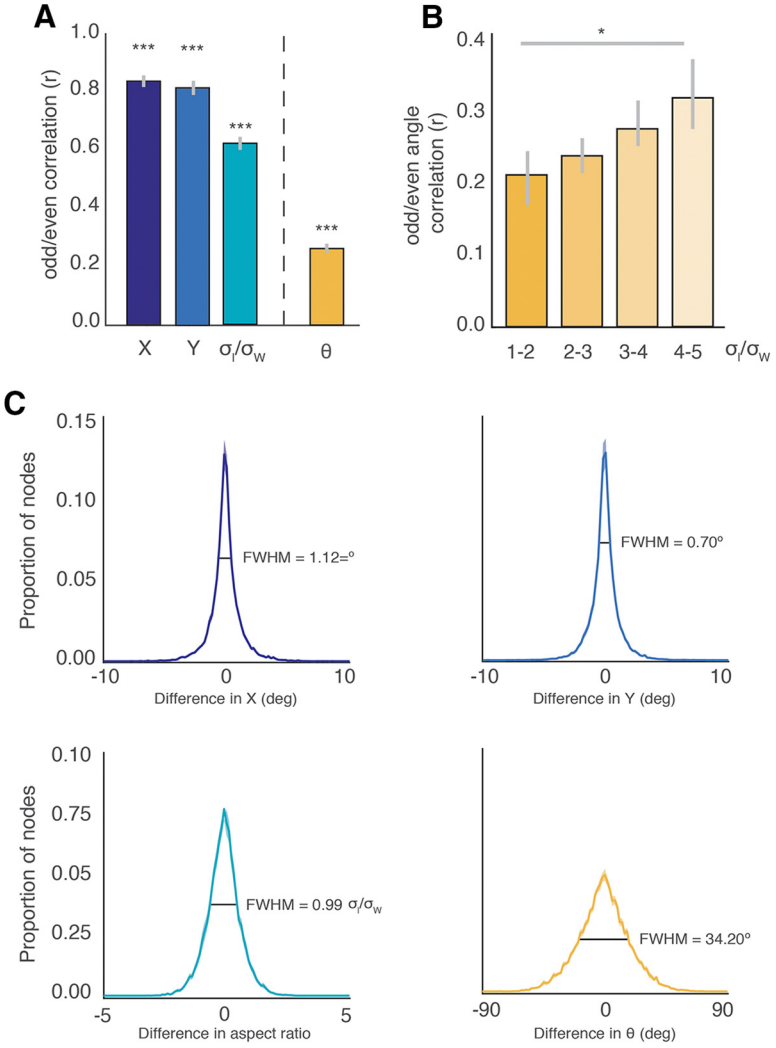

Figure 2. Reliability of the elliptical and oriented pRF model. ***A***, Correlation values derived between independent sets of data for each of the parameters of interest. We observe significant positive correlations for all parameters of interest. The dashed vertical line separates our angle estimate from the other parameters, as this parameter reliability was calculated using a circular correlation method (***$p < 0.001$, relative to zero). ***B***, Reliability of theta estimates as a function of aspect ratio. We tested the prediction that our theta estimates would become increasingly reliable as the aspect ratio increased, as a pRF with an aspect ratio of 1 will result in an unstable theta estimate. As predicted, a one-way repeated-measures ANOVA confirmed that the reliability of our theta estimates increased with increasing aspect ratio (**$p < 0.05$ for the main effect of aspect ratio). ***C***, Distributions of the absolute differences between odd/even runs for each parameter. For each distribution, the FWHM is shown by the black line, with the value given to the right.

Ventral pRFs cover larger area of visual space than dorsal pRFs

Although we observe an increase in aspect ratio for ventral pRFs, it is important to consider the area of visual space covered by these elliptical pRFs. An increase in aspect ratio alone could reflect either elongation of the major axis, but shrinking of the minor axis and thus an overall reduction in area; or elongation of the major axis and an enlarging of overall area. To distinguish between these two possibilities, we calculated the median area in each participant and visual field map, respectively. On average, pRF area was larger in ventral compared with dorsal divisions of EVC (Fig. 5*B*). A three-way repeated-measures ANOVA (VFM, division, and hemisphere) revealed significant main effects of both VFM ($F_{(2,22)} = 37.89$, $p = 7.47^{-8}$) and division ($F_{(1,11)} = 11.30$, $p = 0.006$). However, these main effects are qualified by a significant VFM by division interaction ($F_{(2,22)} = 17.41$, $p = 0.00003$), which highlights that the magnitude of the difference between ventral and dorsal divisions varies across regions. No other interactions were significant ($p > 0.05$, in all cases). Given the nonsignificant main effect of hemisphere ($F_{(1,11)} = 2.22$, $p = 0.16$), pRF area values were averaged across hemispheres. Again, three separate two-way ANOVAs were computed to better interpret the above interaction. These analyses revealed a larger ventral/dorsal difference in V3 compared with both V1 and V2 [V1 to V2; VFM by division ($F_{(1,11)} = 2.35$, $p = 0.15$); V1 to V3, VFM by division ($F_{(1,11)} = 13.40$, $p = 0.004$); V2 to V3, VFM by division ($F_{(1,11)} = 30.48$, $p = 0.0001$)]. Next, we compared directly the pRF area within ventral and dorsal divisions of each visual field map using paired *t* tests (one-tailed). Ventral pRFs covered a significantly larger area of the visual field than dorsal pRFs in V1 and V3 [V1v vs V1d ($t_{(11)} = 3.37$, $p = 0.003$); V3v vs V3d ($t_{(11)} = 4.27$, $p = 0.0005$)], but not V2 (V2v vs V2d ($t_{(11)} = 0.91$, $p = 0.19$),

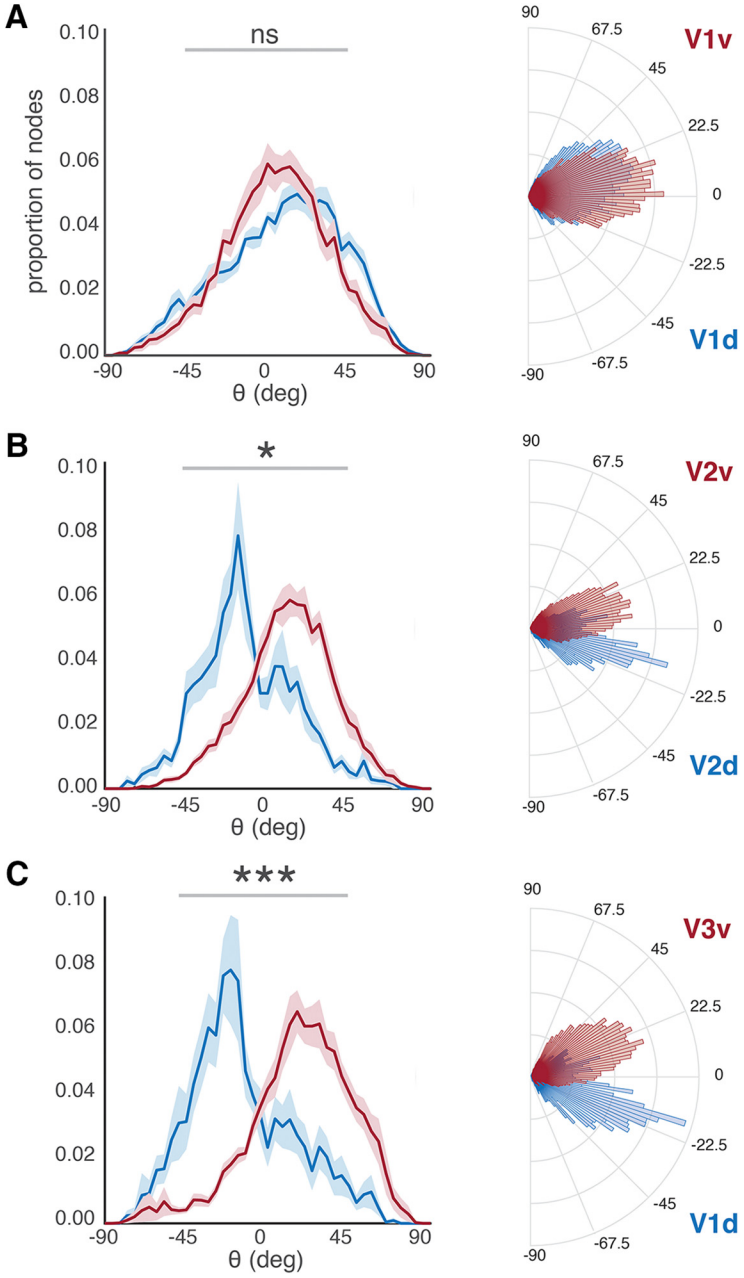

Figure 3. PRF orientation biases in dorsal and ventral divisions of EVC. ***A***, Distributions of pRF orientation in V1d (blue line) and V1v (red line) collapsed across participants and hemispheres. Both distributions appear to be centered largely around zero (horizontal), with little difference in overall bias. The angle histograms of both distributions are plotted to the right. ***B***, Distributions of pRF orientation in V2d (blue line) and V2v (red line) collapsed across participants and hemispheres. V2d exhibits a distribution shifted toward negative orientations, whereas V2v exhibits the opposite bias. These distributions were significantly different from one another (two-sample KS test). The angle histograms of both distributions are plotted to the right and better depict the differential pRF angles in both regions. ***C***, Distributions of pRF orientation in V3d (blue line) and V3v (red line) collapsed across participants and hemispheres. V3d exhibits a distribution shifted toward negative orientations, whereas V3v exhibits the opposite bias. These distributions were significantly different from one another (two-sample KS test). The angle histograms of both distributions are plotted to the right and better depict the differential pRF angles in both regions. $^*p < 0.05$, $^{***}p < 0.001$. The shaded area of each line shows the standard error of the mean (SEM) across participants.

although the numerical increase trended toward significance (Fig. 5*B*).

PRF area and aspect ratio increase with increasing eccentricity

Until now, our analyses have focused on isolated parameters (e.g., angle, aspect ratio, or area), but it is also important to consider the relationship between parameters. It is commonly reported that the size of receptive fields (or pRFs) increases with increasing eccentricity, and that this increase is often linear (Hubel and Wiesel, 1974; Maunsell and Newsome, 1987; Dumoulin and Wandell, 2008; Winawer et al., 2010). Therefore, we investigated the relationship between eccentricity and both pRF area and aspect ratio, which we predicted to show a similar near linear relationship. For each participant and visual field map, we calculated (1) the median area and (2) the median aspect ratio of pRFs in bins of 1° of eccentricity. Next, we computed the average pRF values within each bin collapsing across hemispheres (Fig. 6*A*,*B*).

The largely near linear trend between eccentricity and pRF size reported previously (Dumoulin and Wandell, 2008; Winawer et al., 2010) is evident in both the estimates of pRF area (Fig. 6*A*) and aspect ratio (Fig. 6*B*). Indeed, the general tendency for larger pRFs within successive visual field maps at equal eccentricities is also present for area, with V3 area estimates being larger than those of V2 and V1, respectively (Fig. 6*A*). Notwithstanding differences in absolute aspect ratio (Fig. 6*B*), all regions exhibit a similar near linear relationship whereby aspect ratio increases as a function of eccentricity.

Differential sampling of space between ventral and dorsal divisions of EVC not due to differences in explained variance

While we observe systematic differences between pRFs in ventral and dorsal divisions of EVC, it is important to rule out the possibility that these differences are due to systematic differences in explained variance of our model between these ventral and dorsal divisions. To test this, we calculated the median explained variance in each participant and visual field map, respectively. A three-way repeated-measures ANOVA (VFM, division, and hemisphere) revealed only a significant main effect of VFM ($F_{(2,22)} = 8.241$, $p = 0.002$), reflecting on average the larger explained variance in V3 (mean ± SD: V1 = 0.56 ± 0.08; V2 = 0.59 ± 0.10; V3 = 0.61 ± 0.10). All other main effects and interactions were not significant ($p > 0.05$, in all cases). Thus, the systematic differences reported here between ventral and dorsal divisions of EVC are not due to poorer model fits in one division over the other.

Summary comparison of circular and elliptical pRF models

Finally, to summarize and exemplify the additional information provided by the elliptical pRF model, we calculated the average

pRF parameters (x, y, aspect ratio, and angle) in V2d and V2v (in the left hemisphere) across participants using both circular and elliptical pRF models. A visualization of the resulting average pRFs (Fig. 7) demonstrates the additional information of the elliptical model. In both models, the centers (x, y) of each pRF are largely equivalent, indicating that the addition of parameters for aspect ratio and angle made little difference to the center of the pRF. However, allowing the shape of the pRF to vary not only captures the greater elongation of ventral pRFs, but also demonstrates that this elongation is accompanied by an increase in the area of covered visual field. The orientation of both pRFs toward the fovea is also evident and cannot be captured by a strictly circular model.

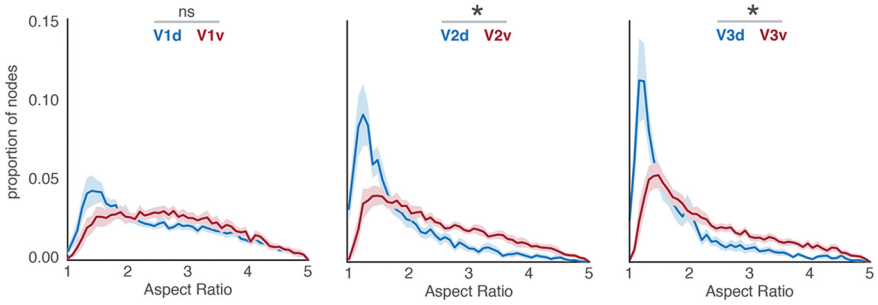

Figure 4. pRF aspect ratio distributions in ventral and dorsal divisions of EVC. Plots depict the average distributions of aspect ratio in each visual field map and division, respectively (blue line, dorsal; red line, ventral). In each case, dorsal distributions are shifted towards smaller aspect ratios. Distributions within each visual field map were compared using two-sample KS tests. In both V2 and V3, ventral and dorsal distributions were significantly different from one another (*$p < 0.05$). The shaded area of each line shows the standard error of the mean (SEM) across participants.

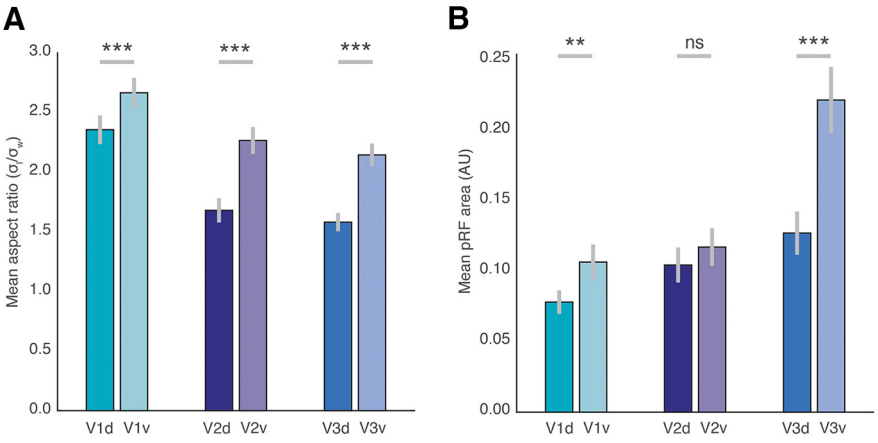

Figure 5. Dorsal versus ventral comparisons. ***A***, Bars represent the mean of the median aspect ratio in each visual field map division collapsed across participants and hemispheres. The pRF aspect ratio was significantly larger within the ventral division of each visual field map (paired t test between dorsal and ventral divisions). ***B***, Bars depict the mean of the median pRF area in each visual field map division collapsed across participants and hemispheres. pRF area was nominally larger in ventral over dorsal V2, and significantly larger in ventral over dorsal V1 and V3 (paired t test between dorsal and ventral divisions). **$p < 0.01$, ***$p < 0.001$. Error bars show the standard error of the mean (SEM) across participants.

Discussion

Using a pRF implementation that models elliptical and oriented pRFs, we demonstrate that ventral and dorsal divisions of EVC differentially sample visual space. First, we demonstrate that pRFs in ventral and dorsal V2 and V3, in particular, are oriented toward the fovea. Second, we highlight that pRFs in ventral divisions of EVC in general exhibit larger aspect ratios and cover a larger area of the visual field than their dorsal counterparts. Third, we show a positive relationship between pRF eccentricity and both the area of covered visual field and the aspect ratio throughout EVC.

The differential sampling of visual space between ventral and dorsal divisions of EVC has implications for visual processing within downstream regions of both the ventral and dorsal pathways, which receive biased inputs from these ventral and dorsal antecedent areas (Kravitz et al., 2013). It is possible that functional differences observed within the ventral and dorsal pathways, such as those for object selectivity ventrally (Kravitz et al., 2013) and attentional allocation dorsally (Danckert and Goodale, 2001), are related to the differences in the sampling of visual space between ventral and dorsal divisions of EVC. It remains an open question whether these differences constrain the functions of downstream areas, are created or strengthened by feedback from those areas, or, most likely, both.

Why do we observe elliptical and oriented pRFs?

Through a cross-validated approach, we demonstrate that our elliptical model captures significantly more of the variance in the time series than the circular model, which has been used widely in the past (Dumoulin and Wandell, 2008; Harvey et al., 2013; Silson et al., 2015, 2016).

Our finding of elliptical pRFs oriented toward the fovea is consistent with prior fMRI findings (Greene et al., 2014) as well as human intracranial recordings (Yoshor et al., 2007).

To understand why we observe elliptical and oriented pRFs, it is important to bear in mind that the pRF for a given voxel will reflect the properties of the individual neurons contributing to that voxel (e.g., receptive field size, orientation) as well as the spatial distribution of those neuronal receptive fields (scatter) and the aggregation function between their activity and the BOLD signal.

First, we consider pRF size. A difference in pRF size between voxels could reflect a difference in the sizes of the receptive fields of individual neurons or a difference in the spatial scatter of those receptive fields. The amount of scatter will be reflected by the cortical magnification factor, which describes the amount of cortex representing a given unit of visual space. The higher the cortical magnification, the less the scatter within a given voxel and the smaller the pRF. It has previously been reported that there are larger cortical activations for stimuli at the lower than at the upper vertical meridian, which is consistent with a difference in cortical magnification (Liu et al., 2006). Further, a recent study (Silva et al., 2017) reported larger cortical magnification factors (smaller pRFs) in representations of the lower visual field (V1d to V3d) than of the upper visual field (V1v to V3v). Such findings are consistent with those of some prior studies in nonhuman primates (Van Essen et al., 1984; Tootell et al., 1988; but see Adams and Horton, 2003) and suggest that the pRF size differences we find between ventral and dorsal divisions of EVC could reflect differences in cortical magnification.

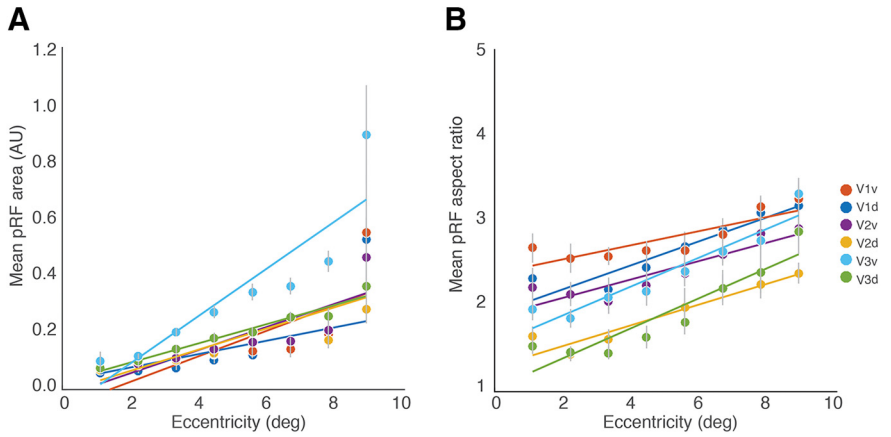

Figure 6. pRF area and aspect ratio increase with eccentricity. ***A***, ***B***, In all visual field maps, pRF area (***A***) and pRF aspect ratio (***B***) increase with eccentricity. The increase in area by hierarchical position (V1, V2, V3) at equal eccentricities is present in ***A*** and is consistent with previous findings that considered pRF size (diameter of circular pRF). Aspect ratio also increases largely linearly with eccentricity (***B***) despite differences in the absolute aspect ratio between visual field maps. In each participant and visual field map, the median surface area and aspect ratio were calculated across nodes in bins of 1° of eccentricity (range, 1° to 9°). Error bars at each eccentricity show the SEM across participants.

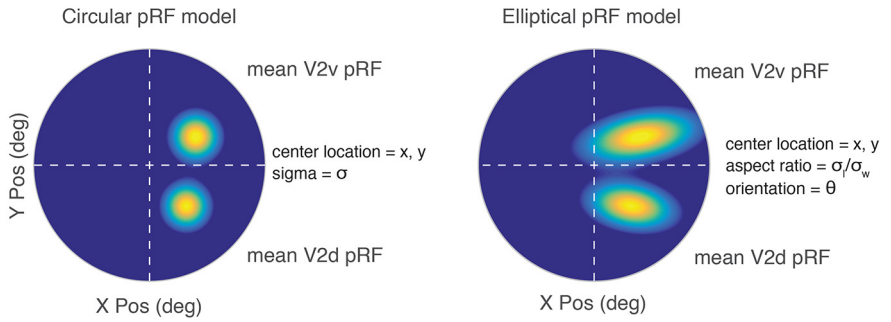

Figure 7. Representation of the information gained from the elliptical pRF model. Left, The average pRF values of all voxels in left V2d and left V2v across participants, derived from the circular pRF model, are plotted on a schematic of the visual field. Right, The average pRF values of all voxels in left V2d and left V2v across participants, derived from the ellipitcal pRF, model are plotted on a schematic of the visual field. Unlike the circular case, the elliptical model captures differences in shape (aspect ratio) and orientation between dorsal and ventral pRFs, which would be unavailable if pRFs were estimated as circles in space.

Second, for aspect ratio, any difference between voxels could reflect the following: (1) anisotropic spatial scatter; 2) a difference in the aspect ratio of the underlying neuronal receptive fields; or (3) differences in the distribution of oriented neuronal receptive fields within voxels. We discuss each of these possibilities in turn.

Anisotropic spatial scatter could result from anisotropy in the sampling of the cortex (i.e., voxel orientation relative to the cortical surface), although systematic differences between ventral and dorsal divisions of EVC seems unlikely. Alternatively, anisotropic spatial scatter could result from anisotropy in cortical magnification. Given that we find that pRFs tend to be oriented toward the fovea, any anisotropy in cortical magnification would have to reflect reduced cortical magnification in the isopolar compared with the isoeccentric dimension, although the prior literature tends to support the opposite (Van Essen et al., 1984, Adams and Horton, 2003; Larsson and Heeger, 2006).

Instead, it is important to note that a consistent finding in the neurophysiological literature is that neuronal receptive fields tend to be oriented in space (Hubel and Wiesel, 1962). Thus, differences in the aspect ratio of the underlying neuronal receptive fields could potentially explain our pRF results. However, a difference in pRF aspect ratio between voxels could also arise from equivalent aspect ratios of the neuronal receptive fields, but from a difference in the angular distribution of those receptive fields across voxels. With our current data, it is hard to tease apart these two possibilities.

Differences between ventral and dorsal divisions of EVC

Our finding of differential sampling of visual space between ventral and dorsal divisions of EVC is consistent with previous evidence demonstrating differences between the processing of information from the upper and lower visual fields. For example, studies of retinal ganglion cell density (Packer et al., 1989; Curcio and Allen, 1990; Curcio et al., 1990) and GABA receptor concentrations in cortex (Eickhoff et al., 2008) demonstrate that these differences are present at even the earliest stages of visual processing.

The larger aspect ratio of pRFs in the ventral division compared with the dorsal division of EVC could reflect a bias for isotropic representations of space dorsally for spatial processing, but also a bias toward an overrepresentation of the fovea ventrally for object and face recognition. For example, as noted earlier, in nonhuman primate inferior temporal cortex neuronal receptive fields tend to overlap the fovea regardless of eccentricity (Op de Beeck and Vogels, 2000), and our results may reflect a similar effect in EVC.

The differences in the orientation we found between dorsal and ventral divisions of EVC could reflect an underlying radial bias (Sasaki et al., 2006; Freeman et al., 2011), although the strength of this radial bias remains disputed (Pratte et al., 2016). Specifically, our analyses demonstrate that the distributions within V2 and V3 peak close to the oblique angle in each quadrant (V2v = 45°, V2d = −36°, V3v = 36°, V3d = −32°).

We did not observe significantly different angle distributions in V1. One potential reason for this is that unlike ventral and dorsal V2 and V3, which are largely anatomically segregated, apart from the difficult-to-map shared central representations of these areas (Schira et al., 2009), our delineation of ventral and dorsal V1 was based on the polar angle of each pRF. It is therefore feasible that the spatial separation between these divisions in V1 is not sufficient enough to detect significant differences in pRF angle. Differences between ventral and dorsal V1 could be further complicated by the vasculature, which likely results in BOLD signals that are pooled from both upper and lower banks of the calcarine sulcus. Future work should systematically compare the orientation selectivity of individual voxels with its pRF orientation and angular position.

Implications for visual processing and future work

The differential sampling of visual space between ventral and dorsal divisions of EVC likely impacts visual processing in high-level regions comprising both ventral and dorsal pathways. For

instance, anterior regions of the dorsal pathway, such as the superior parieto-occipital cortex, which is crucial for guiding hand movements, shows a lower visual field bias (Rossit et al., 2013) that is likely inherited from connections with the dorsal division of EVC (Kravitz et al., 2013). Our data suggest that the dorsal division of EVC exhibits less elongation, as evidenced by smaller aspect ratios, resulting in a more isotropic representation of space (Gattass et al., 2005), which may help explain behavioral advantages for actions such as visually guided pointing in the lower visual field (Danckert and Goodale, 2001). A more isotropic sampling of space in the dorsal division of EVC and the broader dorsal visual pathway likely facilitate the guidance of eye movements and attentional allocation that are thought to reflect dorsal pathway functioning (Goodale et al., 1991; Kravitz et al., 2011), as regions that evenly sample most of visual space are suited ideally to identify items in the visual field that need to be brought into the focus of attention. Whether pRFs in these regions also exhibit similar shapes and orientations as the dorsal division of EVC is a potential avenue for future work.

Although it is intuitive to think that ventral and dorsal divisions of EVC project principally to the ventral and dorsal visual pathways, the neuroanatomy is not as straightforward (Kravitz et al., 2013). Indeed, in humans, category-selective regions considered to comprise the ventral pathway are found in matched pairs on both the lateral and ventral surfaces of occipitotemporal cortex (Kravitz et al., 2010; Silson et al., 2015, 2016) and exhibit differential retinotopic biases that mirror those in ventral and dorsal divisions of EVC, respectively. Although our previous work (Silson et al., 2015, 2016) has focused on the different visual field biases in these areas (e.g., occipital place area—lower visual field, parahippocampal place area—upper visual field), our current data suggest that more focus should be placed upon understanding how these regions sample space within the visual field. Future work could assess the distributions of pRF shape and orientation within these matched category-selective regions, which may inform the specific computations each region performs.

Conclusion

Together, our data suggest systematic differences in the sampling of space between ventral and dorsal divisions of EVC. The differential sampling of space is consistent with previous differences between the upper and lower representations of the visual field at both retinal and cortical levels, and likely contribute to and/or stem from the functional differentiation of visual processing observed in higher-level regions of the ventral and dorsal cortical visual pathways.

References

Adams DL, Horton JC (2003) A precise retinotopic map of primate striate cortex generated from the representation of angioscotomas. J Neurosci 23:3771–3789. Medline

Arcaro MJ, McMains SA, Singer BD, Kastner S (2009) Retinotopic organization of human ventral visual cortex. J Neurosci 29:10638–10652. CrossRef Medline

Cox RW (1996) AFNI: software for analysis and visualization of functional magnetic resonance neuroimages. Computers and Biomedical research, 29(3), 162–173.

Curcio CA, Allen KA (1990) Topography of ganglion cells in human retina. J Comp Neurol 300:5–25. CrossRef Medline

Curcio CA, Sloan KR, Kalina RE, Hendrickson AE (1990) Human photoreceptor topography. J Comp Neurol 292:497–523. CrossRef Medline

Danckert J, Goodale MA (2001) Superior performance for visually guided pointing in the lower visual field. Exp Brain Res 137:303–308. CrossRef Medline

DeYoe EA, Bandettini P, Neitz J, Miller D, Winans P (1994) Functional magnetic resonance imaging (FMRI) of the human brain. J Neurosci Methods 54:171–187. CrossRef Medline

Dumoulin SO, Wandell BA (2008) Population receptive field estimates in human visual cortex. Neuroimage 39:647–660. CrossRef Medline

Eickhoff SB, Rottschy C, Kujovic M, Palomero-Gallagher N, Zilles K (2008) Organizational principles of human visual cortex revealed by receptor mapping. Cereb Cortex 18:2637–2645. CrossRef Medline

Engel SA, Glover GH, Wandell BA (1997) Retinotopic organization in human visual cortex and the spatial precision of functional MRI. Cereb Cortex 7:181–192. CrossRef Medline

Fortenbaugh FC, Silver MA, Robertson LC (2015) Individual differences in visual field shape modulate the effects of attention on the lower visual field advantage in crowding. J Vis 15(2):19, 1–15. CrossRef Medline

Freeman J, Brouwer GJ, Heeger DJ, Merriam EP (2011) Orientation decoding depends on maps, not columns. J Neurosci 31:4792–4804. CrossRef Medline

Gattass R, Nascimento-Silva S, Soares JG, Lima B, Jansen AK, Diogo AC, Farias MF, Botelho MM, Mariani OS, Azzi J, Fiorani M (2005) Cortical visual areas in monkeys: location, topography, connections, columns, plasticity and cortical dynamics. Philos Trans R Soc Lond B Biol Sci 360:709–731. CrossRef Medline

Genzano VR, Di Nocera F, Ferlazzo F (2001) Upper/lower visual field asymmetry on a spatial relocation memory task. Neuroreport 12:1227–1230. CrossRef Medline

Goodale MA, Milner AD, Jakobson LS, Carey DP (1991) A neurological dissociation between perceiving objects and grasping them. Nature 349:154–156. CrossRef Medline

Greene CA, Dumoulin SO, Harvey BM, Ress D (2014) Measurement of population receptive fields in human early visual cortex using back-projection tomography. J Vis 14(1):17, 1–17. CrossRef Medline

Harvey BM, Klein BP, Petridou N, Dumoulin SO (2013) Topographic representation of numerosity in the human parietal cortex. Science 341:1123–1126. CrossRef Medline

He S, Cavanagh P, Intriligator J (1996) Attentional resolution and the locus of visual awareness. Nature 383:334–337. CrossRef Medline

Hubel DH, Wiesel TN (1962) Receptive fields, binocular interaction and functional architecture in the cat's visual cortex. J Physiol 160:106–154. CrossRef Medline

Hubel DH, Wiesel TN (1974) Uniformity of monkey striate cortex: a parallel relationship between field size, scatter, and magnification factor. J Comp Neurol 158:295–305. CrossRef Medline

Kay KN, Winawer J, Mezer A, Wandell BA (2013) Compressive spatial summation in human visual cortex. J Neurophysiol 110:481–494. CrossRef Medline

Kravitz DJ, Kriegeskorte N, Baker CI (2010) High-level visual object representations are constrained by position. Cereb Cortex 20:2916–2925. CrossRef Medline

Kravitz DJ, Peng CS, Baker, CI (2011) Real-world scene representations in high-level visual cortex: it's the spaces more than the places. Journal of Neuroscience, 31(20), 7322–7333.

Kravitz DJ, Saleem KS, Baker CI, Ungerleider LG, Mishkin M (2013) The ventral visual pathway: an expanded neural framework for the processing of object quality. Trends Cogn Sci 17:26–49. CrossRef Medline

Larsson J, Heeger DJ (2006) Two retinotopic visual areas in human lateral occipital cortex. Journal of Neuroscience, 26(51), 13128–13142.

Levine MW, McAnany JJ (2005) The relative capabilities of the upper and lower visual hemifields. Vision Res 45:2820–2830. CrossRef Medline

Liu T, Heeger DJ, Carrasco M (2006) Neural correlates of the visual vertical meridian asymmetry. J Vis 6(11):12, 1294–1306 CrossRef Medline

Maunsell JH, Newsome WT (1987) Visual processing in monkey extrastriate cortex. Annu Rev Neurosci 10:363–401. CrossRef Medline

Op De Beeck H, Vogels R (2000) Spatial sensitivity of macaque inferior temporal neurons. J Comp Neurol 426:505–518. CrossRef Medline

Packer O, Hendrickson AE, Curcio CA (1989) Photoreceptor topography of the retina in the adult pigtail macaque (Macaca nemestrina). J Comp Neurol 288:165–183. CrossRef Medline

Pratte MS, Sy JL, Swisher JD, Tong F (2016) Radial bias is not necessary for orientation decoding. NeuroImage, 127, 23–33.

Rossit S, McAdam T, McLean DA, Goodale MA, Culham JC (2013) fMRI reveals a lower visual field preference for hand actions in human superior parieto-occipital cortex (SPOC) and precuneus. Cortex 49:2525–2541. CrossRef Medline

Rutkowski JS, Crewther DP, Crewther SG (2002) Normal readers have an

upper visual field advantage in change detection. Clin Exp Ophthalmol 30:227–330. CrossRef Medline

Sasaki Y, Rajimehr R, Kim BW, Ekstrom LB, Vanduffel W, Tootell RB (2006) The radial bias: a different slant on visual orientation sensitivity in human and nonhuman primates. Neuron 51:661–670. CrossRef Medline

Schira MM, Tyler CW, Breakspear M, Spehar B (2009) The foveal confluence in human visual cortex. J Neurosci 29:9050–9058. CrossRef Medline

Sereno M, Dale AM, Reppas JB, Kwong KK, Belliveau JW, Brady TJ, Rosen BR, Tootell RBH (1995) Borders of multiple visual areas in humans revealed by functional magnetic resonance imaging. Science 268:889–893. CrossRef Medline

Sheth BR, Young R (2016) Two visual pathways in primates based on sampling of space: exploitation and exploration of visual information. Front Integr Neurosci 10:37. CrossRef Medline

Silson EH, Chan AW, Reynolds RC, Kravitz DJ, Baker CI (2015) A retinotopic basis for the division of high-level scene processing between lateral and ventral human occipitotemporal cortex. J Neurosci 35:11921–11935. CrossRef Medline

Silson EH, Groen II, Kravitz DJ, Baker CI (2016) Evaluating the correspondence between face-, scene-, and object-selectivity and retinotopic organization within lateral occipitotemporal cortex. J Vis 16(6):14, 1–21. CrossRef Medline

Silva MF, Brascamp JW, Ferreira S, Castelo-Branco M, Dumoulin SO, Harvey BM (2017) Radial asymmetries in population receptive field size and cortical magnification factor in early visual cortex. Neuroimage 167:41–52. CrossRef Medline

Tootell RB, Switkes E, Silverman MS, Hamilton SL (1988) Functional anatomy of macaque striate cortex. II. Retinotopic organization. J Neurosci 8:1531–1568. Medline

Van Essen DC, Newsome WT, Maunsell JH (1984) The visual field representation in striate cortex of the macaque monkey: asymmetries, anisotropies, and individual variability. Vision Res 24:429–448. CrossRef Medline

Wandell BA, Dumoulin SO, Brewer AA (2007) Visual field maps in human cortex. Neuron 56:366–383. CrossRef Medline

Winawer J, Horiguchi H, Sayres RA, Amano K, Wandell BA (2010) Mapping hV4 and ventral occipital cortex: the venous eclipse. J Vis 10(5):1, 1–22. CrossRef Medline

Yoshor D, Bosking WH, Ghose GM, Maunsell JH (2007) Receptive fields in human visual cortex mapped with surface electrodes. Cereb Cortex 17: 2293–2302. CrossRef Medline

Zuiderbaan W, Harvey BM, Dumoulin SO (2012) Modeling center-surround configurations in population receptive fields using fMRI. J Vis 12(3):10, 1–15. CrossRef Medline